



**HAL**  
open science

# Inter-subject registration and application of the SIGMA rat brain atlas for regional labeling in functional ultrasound imaging

Benjamin Vidal, Marine Droguerre, Ludovic Venet, Marco Valdebenito, Franck Mouthon, Luc Zimmer, Mathieu Charvériat

## ► To cite this version:

Benjamin Vidal, Marine Droguerre, Ludovic Venet, Marco Valdebenito, Franck Mouthon, et al.. Inter-subject registration and application of the SIGMA rat brain atlas for regional labeling in functional ultrasound imaging. *Journal of Neuroscience Methods*, 2021, 355, pp.109139. 10.1016/j.jneumeth.2021.109139 . hal-04763118

**HAL Id: hal-04763118**

**<https://hal.science/hal-04763118v1>**

Submitted on 13 Nov 2024

**HAL** is a multi-disciplinary open access archive for the deposit and dissemination of scientific research documents, whether they are published or not. The documents may come from teaching and research institutions in France or abroad, or from public or private research centers.

L'archive ouverte pluridisciplinaire **HAL**, est destinée au dépôt et à la diffusion de documents scientifiques de niveau recherche, publiés ou non, émanant des établissements d'enseignement et de recherche français ou étrangers, des laboratoires publics ou privés.



Distributed under a Creative Commons Attribution - NonCommercial 4.0 International License

SHORT COMMUNICATION

1  
2  
3  
4  
5  
6  
7  
8  
9  
10  
11  
12  
13

**Inter-subject registration and application of the SIGMA rat brain atlas for regional labeling in functional ultrasound imaging**

Benjamin Vidal<sup>1,2#\*</sup>, Marine Droguerre<sup>1#</sup>, Ludovic Venet<sup>1</sup>, Marco Valdebenito<sup>3</sup>, Franck Mouthon<sup>1</sup>, Luc Zimmer<sup>2,3,4</sup>, Mathieu Charvériat<sup>1</sup>

- <sup>1</sup> Theranexus, Lyon, France
- <sup>2</sup> Lyon Neuroscience Research Center, Bron, France
- <sup>3</sup> CERMEP-Université Lyon 1, Lyon, France
- <sup>4</sup> Hospices Civils de Lyon, Lyon, France
- # Both authors contributed equally

**\* Correspondence**

Dr Benjamin VIDAL  
CERMEP – Imagerie du vivant  
59, Boulevard Pinel, 69677 Bron, France  
Mail : benjamin.vidal@theranexus.fr

## 20 **Abstract**

21 Background: Recent advances using functional ultrasound (fUS) imaging have opened new  
22 avenues to evaluate brain activity through the regional monitoring of cerebral blood volume  
23 (CBV) dynamics. In particular, this technology paves the way for understanding physiological  
24 or pathological cerebral processes or exploring the pharmacological profiles of new drugs  
25 targeting brain disorders. One of the main difficulties of this technology is the lack of  
26 standardized and validated tools, in particular relevant brain atlases, to help improving the  
27 accuracy, automation and reproducibility of fUS data analysis. New method: Here, we  
28 demonstrate the possibility to use the MRI-validated SIGMA brain atlas in rat to perform fast  
29 and precise analysis of CBV changes in numerous functionally relevant regions of interest  
30 using fUS imaging. We applied this atlas to a dataset obtained in anesthetized rats evaluating  
31 the cerebral effects of atomoxetine, a norepinephrine reuptake inhibitor currently marketed in  
32 attention-deficit/hyperactivity-disorder. Results: This approach enabled to show the  
33 subregional effects of atomoxetine in the rat with very few inter-individual differences in  
34 some areas, such as the dentate gyrus. Conclusions: We show the feasibility of inter-  
35 individual registration of 2D phar-maco-fUS data and subsequent detailed analysis using the  
36 SIGMA atlas.

37

## 38 **1. Introduction**

39 The last years have seen the emergence of functional ultrasound (fUS) imaging, a new  
40 functional neuroimaging tool (Macé et al., 2011), which enables the imaging of brain activity  
41 through the regional monitoring of cerebral blood volume (CBV) dynamics based on  
42 neurovascular coupling. fUS imaging is characterized by a high spatiotemporal resolution and  
43 sensitivity, along with a high portability as compared to functional magnetic resonance  
44 imaging (fMRI). In rodents, fUS offers the possibility to investigate brain activity at a spatial  
45 resolution of about 100  $\mu\text{m}$  from the upper layers of the cortex to the deepest brain structures.  
46 A small number of studies have confirmed the interest of this technology to monitor the effect  
47 of pharmacological molecules (Rabut et al., 2020; Vidal et al., 2020a, 2020b). There is a need  
48 for a standardized atlas that would enable the precise delineation of relevant regions of  
49 interest, rather than manually drawing the different regions on each individual scan, in order  
50 to improve the accuracy and reproducibility of fUS data analysis.

51 In a recent study, Barrière and collaborators (Barrière et al., 2019) developed a complete set  
52 of MRI references and resources (SIGMA rat brain atlas), compatible with common  
53 neuroimaging software and enabling researchers to perform unified analyses of both structural  
54 and functional data from MRI.

55 In this study, we present for the first time the feasibility to register different sessions of fUS  
56 data in the same space before using the SIGMA rat brain atlas, to perform fast measurement  
57 of CBV changes in numerous functionally relevant regions of interest using fUS imaging. We  
58 adapted this atlas to a dataset obtained in a phar-maco-fUS study in anesthetized rats  
59 evaluating the cerebral effects of atomoxetine, a norepinephrine reuptake inhibitor currently  
60 marketed in attention-deficit/hyperactivity-disorder (ADHD).

61

## 62 **2. Materials and methods**

### 63 **2.1 Animals**

64 Wistar-Kyoto (8-week old) male rats were purchased from Janvier labs (France) and  
65 maintained under controlled environmental conditions (12/12 h light-dark cycle,  $22 \pm 1^\circ\text{C}$   
66 ambient temperature) with food and water ad libitum. Animal surgery and experimentations  
67 were conducted in strict accordance with the recommendations and guidelines of the  
68 European Union (Directive 2010/63/EU) and strictly followed the policies of the French ethic  
69 committee for preclinical research. Procedures and protocols herein described were authorized  
70 by the French Ministry of Research (authorization reference: APAFIS19829). All efforts were  
71 made to improve animal welfare and minimize animal sufferings.

72

### 73 ***2.2 Drugs and administration procedures***

74 Atomoxetine (Sigma-Aldrich) was dissolved in saline and administered intraperitoneally (2  
75 mL/kg) at 1 mg/kg (n=3). For the control group, only saline was administered at the same  
76 volume (n = 4).

77

### 78 ***2.3 Surgical preparation***

79 One day prior to ultrasound imaging, a thin-skulled surgery was performed under isoflurane  
80 (induction 4% for the first minutes, lowered to 2% in 1 L/min for constant anesthesia) and  
81 with subcutaneous buprenorphine (0.05 mg/kg; (Buprecare, Axience)) pretreatment. After  
82 shaving and cleaning with betadine, the scalp was incised to visualize the lateral sides of the  
83 skull from the bregma to the lambda anatomical landmarks. The bone was thinned from -3.00  
84 mm to -7.00 mm (AP) and +5.00 to -5.00 mm (L) from bregma using a drill at low speed with  
85 a micro drill steel burr (Harvard Apparatus, 75-1887). Saline was frequently added between  
86 drilling sessions to avoid drought and overheating. When the skull was thin enough to be  
87 flexible, the scalp was sutured, betadine and lidocaine were locally applied and the rats were  
88 allowed to recover from anesthesia.

89

### 90 ***2.4 Functional ultrasound imaging***

91 Thin-skulled rats were anesthetized with isoflurane, placed in a stereotaxic frame and sutures  
92 were removed to expose the thin-skulled window. Rats were scanned using a system  
93 dedicated to small animal ultrasound neuroimaging (Iconeus, Paris, France). An  
94 intraperitoneal catheter was placed for atomoxetine injection during the scan. During the  
95 imaging session, body temperature was rectally monitored and maintained using a heating  
96 blanket, and respiratory and heart rates were also continuously monitored (TCMT, Minerve,  
97 France). Using the Ultrafast Compound Doppler Imaging technique (Bercoff et al., 2011) and  
98 real-time filtering with Singular Value Decomposition (Demené et al., 2015), high resolution  
99 Doppler vascular images were acquired every second during 15 min at bregma -5.3 mm (Fig.  
100 1A), with an injection (atomoxetine or saline) performed at 5 min of acquisition.

101 Before data processing, all fUS acquisitions were automatically registered together in Matlab  
102 on a custom fUS template. This template was obtained by computing the mean pixel-by-pixel  
103 image of all acquisitions from the whole dataset, generating a first mean reference image that  
104 reflected the gross anatomical properties of the unregistered images. Linear registration of  
105 each single initial acquisition was then performed on this global mean reference image. An  
106 additional, second, mean image of all those registered acquisitions was computed to generate  
107 a new template, which was improved in quality compared to the first (as images were roughly

108 registered together). Linear registration of all initial unregistered acquisitions was performed  
109 again on this new template, before averaging the newly registered images in order to generate  
110 a third template that was further optimized compared to the previous iteration (as images were  
111 better registered since the reference template was improved). These steps were repeated for  
112 several iterations until there was no residual difference between 2 successive means, meaning  
113 that the optimal template was obtained (reflecting the global common anatomical properties  
114 between acquisitions). All fUS acquisitions were then registered on this final template using  
115 linear registration before non-linear registration using the Demons algorithm (Pennec et al.,  
116 1999) with a Gaussian smoothing applied on the vector field to only match the global shapes  
117 of the images without focusing on the small vessels. This registration method was estimated  
118 on the denoised images, obtained after singular value decomposition (SVD) of each fUS  
119 acquisition to keep the first component only (enabling to reduce the influence of small  
120 artifacts and noise to focus on the important anatomical properties of each acquisition for the  
121 calculation), and applied to the original data. The registered data were then temporally filtered  
122 (lowpass filter and highpass filter with respective cutoff frequencies of 0.1 Hz and 0.0008  
123 Hz).

124 The corresponding 2D slice of interest was then extracted from the SIGMA atlas (-5.3 mm  
125 from bregma, with a nearest neighbor interpolation in order to keep whole number values for  
126 each label) and coregistered on the fUS template using manual transformations in the ITK-  
127 Snap software, until the boundaries of the cortex and bottom of the brain matched those from  
128 the template (Fig. 1B). The Power Doppler signal was then automatically extracted from each  
129 region for each individual scan using a Matlab script and normalized to the baseline (between  
130 0 and 5 minutes), enabling the measurement of the relative cerebral blood volume (rCBV)  
131 changes occurring after injection of saline or atomoxetine in the different ROIs (Fig. 1C). For  
132 the functional connectivity analysis, the temporal correlation between the different pairs of  
133 ROIs was estimated using the dedicated software available with the Iconeus system. The  
134 difference between atomoxetine and saline for rCBV (Fig. 2A-B) and functional connectivity  
135 (Fig. 2C) changes was calculated in each region.

136

### 137 **3. Results**

138 This mapping showed that atomoxetine effects on rCBV differed across cortical areas, with  
139 important CBV increases in the dysgranular retrosplenial cortex and the primary visual cortex  
140 (maximal increases of +15% and +18% respectively), but limited changes in the granular  
141 retrosplenial cortex (+3.5% in part B - see Fig. 1C and 2A-B). Similarly, in the hippocampus,  
142 atomoxetine effects were highest in the dentate gyrus (+8.5%) and CA1 (+3%) and absent in  
143 CA2. In the midbrain, the superficial and deep parts of the superior colliculus displayed  
144 pronounced CBV increases following atomoxetine administration, whereas the periaqueductal  
145 gray was not impacted. Alternatively, time-dependent brain activation can be summarized as  
146 depicted in Fig. 2A (differences between atomoxetine and saline groups). As compared to  
147 saline injection, atomoxetine also had complex and various effects on the functional  
148 connectivity (Fig. 2C).

149

### 150 **4. Discussion**

151 Here we show that the SIGMA atlas is a valuable tool to label fUS images after registration of  
152 the data in the same space as the corresponding 2D slices from the atlas, without possible bias  
153 induced by the user's definition of ROIs. This is particularly relevant in pharmaco-fUS  
154 experiments, as drug effect can be complex and variable across regions, as illustrated here  
155 with atomoxetine. The effects of atomoxetine 1 mg/kg have been previously evaluated using  
156 large manually defined ROIs such as the visual cortex, the thalamus and the hippocampus  
157 (Vidal et al., 2020b). As an example in this last region, the current study confirms this impact  
158 but more importantly, at sub-regional resolution, suggests that the dentate gyrus and CA1 are  
159 more largely affected than CA3, and CA2 is not impacted. When a large ROI was used to  
160 define the hippocampus, we found rather subtle changes of CBV at this dose (maximal change  
161 of +4%) in our previous study (Vidal et al., 2020b), whereas the present results highlight the  
162 dentate gyrus as one of the most important area in the effect of atomoxetine. Another example  
163 is the case of the retrosplenial cortex, with a strong CBV increase in the dysgranular part and  
164 almost no effect in the granular part. In our previous study, we found a global maximal  
165 increase of 13% in this area with however no indication of the subregional specific effect of  
166 atomoxetine (Vidal et al., 2020b). This illustrates how a molecule can impact differently  
167 subregions of the same area and shows the importance of taking such subregions into account  
168 when analyzing fUS data. These results are consistent with the known strikingly different  
169 functional roles of granular and dysgranular retrosplenial cortices (Pothuizen et al., 2009) and  
170 are therefore of relevance to understand the effect of atomoxetine.

171 The aim of the present work was to provide a simplified method for performing group  
172 analysis of fUS data, without the need of additional morphological data. The manual  
173 registration of the atlas on the final template, although more robust than performing manual  
174 definition of ROIs/manual registration of an atlas on each individual data, constitutes a limit.  
175 One would replace such manual step by using additional angiography MRI data and their  
176 corresponding anatomic MRI images that could be registered on the MRI Sigma anatomical  
177 template, making the link between vascular and anatomic images.

178 As described in Barriere et al., 2019, the particular interest of the SIGMA anatomical atlas is  
179 to merge together two distinct 3D rat brain atlases, the Waxholm (Papp et al., 2014) and the  
180 Tohoku (Valdés-Hernández et al., 2011) atlases, enabling full brain coverage with a strong  
181 emphasis on both the cortical areas (provided by the Tohoku atlas) and the subcortical areas  
182 (provided by the Waxholm atlas). In comparison, other resources do not provide full brain  
183 coverage which such details, or are unavailable in a format compatible with the usual  
184 neuroimaging softwares. Previous fUS studies used the Paxinos atlas to delineate the regions  
185 of interest in 2D (Mairesse et al., 2019; Osmanski et al., 2014; Rahal et al., 2020), which  
186 provides a high precision on the different areas without offering the possibility of analyzing  
187 3D data. Conversely, the SIGMA atlas could be used on 3D fUS data, either acquired  
188 simultaneously (as in (Rabut et al., 2019), which used separately the Waxholm and Tohoku  
189 atlases on the same data) or by imaging successive slices using a motorized probe (as in  
190 (Gesnik et al., 2017).

191 As a perspective, the use of SIGMA atlas can be considered as an elegant tool to compare  
192 data from multimodal MRI and fUS, further reinforcing reproducibility and confidence in  
193 non-clinical neuroimaging studies, but also providing an answer to the recently underlined

194 potential of fUS to be hybridized with those other neuro-imaging modalities such as positron  
195 emission tomography (Tournier et al., 2020).

196

## 197 **Contributions**

198 BV and MV performed the fUS experiments. BV and LV analyzed the data. MD and MC  
199 designed the experiments and managed the project. BV, MD and MC wrote the first draft.  
200 MD, BV, LZ, FM, MC reviewed the article. All authors approved the final manuscript.

201

## 202 **Data availability**

203 The Matlab scripts and data are available upon reasonable request.

204

## 205 **Competing interests**

206 This work was supported by Theranexus Company. MD, BV, LV, FM and MC are full-time  
207 employees of Theranexus company. The other authors (LZ and MV) declare no financial  
208 conflict of interest.

209

## 210 **References**

- 211 Barrière, D.A., Magalhães, R., Novais, A., Marques, P., Selingue, E., Geffroy, F., Marques,  
212 F., Cerqueira, J., Sousa, J.C., Boumezbeur, F., Bottlaender, M., Jay, T.M., Cachia, A.,  
213 Sousa, N., Mériaux, S., 2019. The SIGMA rat brain templates and atlases for multimodal  
214 MRI data analysis and visualization. *Nat. Commun.* <https://doi.org/10.1038/s41467-019-13575-7>
- 216 Bercoff, J., Montaldo, G., Loupas, T., Savery, D., Mézière, F., Fink, M., Tanter, M., 2011.  
217 Ultrafast compound doppler imaging: Providing full blood flow characterization. *IEEE*  
218 *Trans. Ultrason. Ferroelectr. Freq. Control.* <https://doi.org/10.1109/TUFFC.2011.1780>
- 219 Demené, C., Deffieux, T., Pernot, M., Osmanski, B.F., Biran, V., Gennisson, J.L., Sieu, L.A.,  
220 Bergel, A., Franqui, S., Correas, J.M., Cohen, I., Baud, O., Tanter, M., 2015.  
221 Spatiotemporal Clutter Filtering of Ultrafast Ultrasound Data Highly Increases Doppler  
222 and fUltrasound Sensitivity. *IEEE Trans. Med. Imaging.*  
223 <https://doi.org/10.1109/TMI.2015.2428634>
- 224 Gesnik, M., Blaize, K., Deffieux, T., Gennisson, J.L., Sahel, J.A., Fink, M., Picaud, S.,  
225 Tanter, M., 2017. 3D functional ultrasound imaging of the cerebral visual system in  
226 rodents. *Neuroimage.* <https://doi.org/10.1016/j.neuroimage.2017.01.071>
- 227 Macé, E., Montaldo, G., Cohen, I., Baulac, M., Fink, M., Tanter, M., 2011. Functional  
228 ultrasound imaging of the brain. *Nat. Methods.* <https://doi.org/10.1038/nmeth.1641>
- 229 Mairesse, J., Zinni, M., Pansiot, J., Hassan-Abdi, R., Demene, C., Colella, M., Charriaud-  
230 Marlangue, C., Rideau Batista Novais, A., Tanter, M., Maccari, S., Gressens, P.,  
231 Vaiman, D., Soussi-Yanicostas, N., Baud, O., 2019. Oxytocin receptor agonist reduces  
232 perinatal brain damage by targeting microglia. *Glia.* <https://doi.org/10.1002/glia.23546>
- 233 Osmanski, B.F., Pezet, S., Ricobaraza, A., Lenkei, Z., Tanter, M., 2014. Functional ultrasound  
234 imaging of intrinsic connectivity in the living rat brain with high spatiotemporal  
235 resolution. *Nat. Commun.* <https://doi.org/10.1038/ncomms6023>
- 236 Papp, E.A., Leergaard, T.B., Calabrese, E., Johnson, G.A., Bjaalie, J.G., 2014. Waxholm  
237 Space atlas of the Sprague Dawley rat brain. *Neuroimage.*  
238 <https://doi.org/10.1016/j.neuroimage.2014.04.001>
- 239 Pennec, X., Cachier, P., Ayache, N., 1999. Understanding the “demon’s algorithm”: 3D non-  
240 rigid registration by gradient descent, in: *Lecture Notes in Computer Science (Including*

241 Subseries Lecture Notes in Artificial Intelligence and Lecture Notes in Bioinformatics).  
242 [https://doi.org/10.1007/10704282\\_64](https://doi.org/10.1007/10704282_64)

243 Pothuizen, H.H.J., Davies, M., Albasser, M.M., Aggleton, J.P., Vann, S.D., 2009. Granular  
244 and dysgranular retrosplenial cortices provide qualitatively different contributions to  
245 spatial working memory: Evidence from immediate-early gene imaging in rats. *Eur. J.*  
246 *Neurosci.* <https://doi.org/10.1111/j.1460-9568.2009.06881.x>

247 Rabut, C., Correia, M., Finel, V., Pezet, S., Pernot, M., Deffieux, T., Tanter, M., 2019. 4D  
248 functional ultrasound imaging of whole-brain activity in rodents. *Nat. Methods.*  
249 <https://doi.org/10.1038/s41592-019-0572-y>

250 Rabut, C., Ferrier, J., Bertolo, A., Osmanski, B., Mousset, X., Pezet, S., Deffieux, T., Lenkei,  
251 Z., Tanter, M., 2020. PharmacofUS: Quantification of pharmacologically-induced  
252 dynamic changes in brain perfusion and connectivity by functional ultrasound imaging in  
253 awake mice. *Neuroimage.* <https://doi.org/10.1016/j.neuroimage.2020.117231>

254 Rahal, L., Thibaut, M., Rivals, I., Claron, J., Lenkei, Z., Sitt, J.D., Tanter, M., Pezet, S., 2020.  
255 Ultrafast ultrasound imaging pattern analysis reveals distinctive dynamic brain states and  
256 potent sub-network alterations in arthritic animals. *Sci. Rep.*  
257 <https://doi.org/10.1038/s41598-020-66967-x>

258 Tournier, N., Comtat, C., Lebon, V., Gennisson, J.L., 2020. Challenges and Perspectives of  
259 the Hybridization of PET with Functional MRI or Ultrasound for Neuroimaging.  
260 *Neuroscience.* <https://doi.org/10.1016/j.neuroscience.2020.10.015>

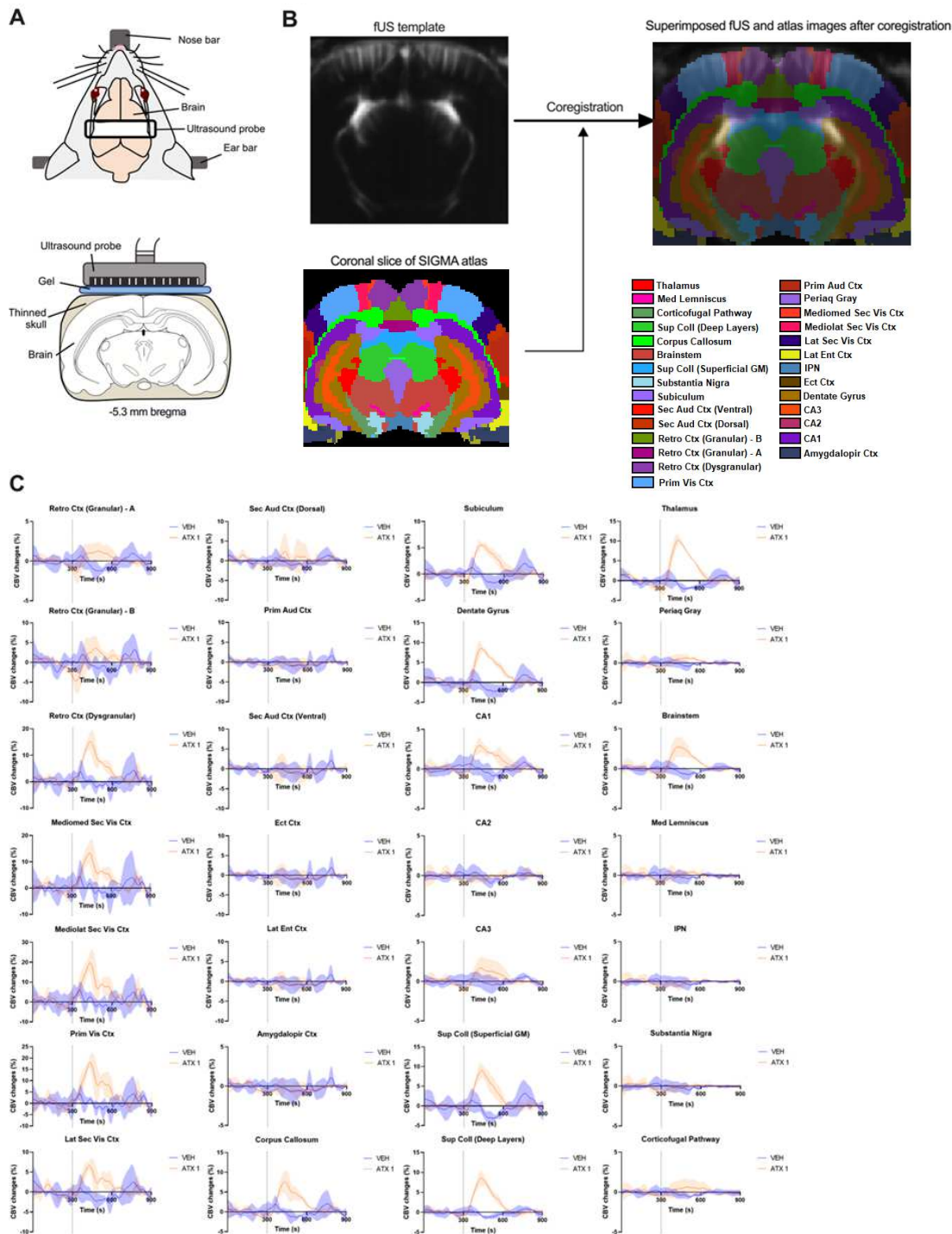
261 Valdés-Hernández, P.A., Sumiyoshi, A., Nonaka, H., Haga, R., Aubert-Vásquez, E., Ogawa,  
262 T., Iturria-Medina, Y., Riera, J.J., Kawashima, R., 2011. An in vivo MRI template set for  
263 morphometry, tissue segmentation, and fMRI localization in rats. *Front. Neuroinform.*  
264 <https://doi.org/10.3389/fninf.2011.00026>

265 Vidal, B., Droguerre, M., Valdebenito, M., Zimmer, L., Hamon, M., Mouthon, F., Charvériat,  
266 M., 2020a. PharmacofUS for Characterizing Drugs for Alzheimer's Disease – The Case  
267 of THN201, a Drug Combination of Donepezil Plus Mefloquine. *Front. Neurosci.*  
268 <https://doi.org/10.3389/fnins.2020.00835>

269 Vidal, B., Droguerre, M., Venet, L., Zimmer, L., Valdebenito, M., Mouthon, F., Charvériat,  
270 M., 2020b. Functional ultrasound imaging to study brain dynamics: Application of  
271 pharmacofUS to atomoxetine. *Neuropharmacology.*  
272 <https://doi.org/10.1016/j.neuropharm.2020.108273>

273  
274

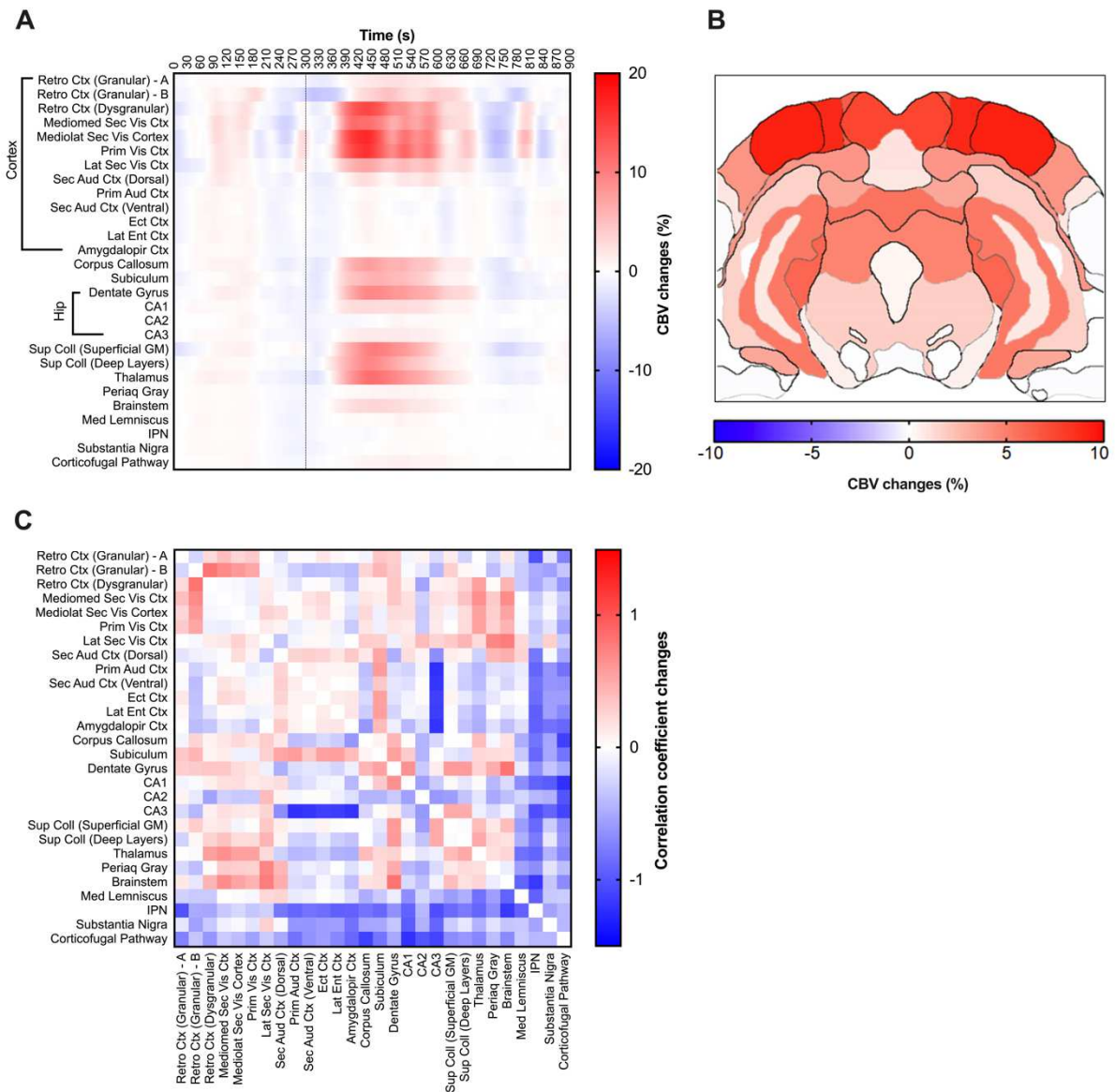




276  
277  
278  
279  
280  
281  
282  
283  
284

**Fig. 1: Precise mapping of atomoxetine impact on CBV using the SIGMA rat brain atlas**  
 (A) Schematic representation of the experimental setup during fUS imaging (up) and fUS probe position in a coronal brain plan (down). (B) Steps involved in coregistration between the 2D slice of interest from the SIGMA atlas and the fUS template. (C) rCBV changes after saline or atomoxetine administration in the different brain ROIs. The injection time is shown by a dashed line. ATX: atomoxetine; Aud: Auditory; CA1, CA2, CA3: cornu ammonis areas; CBV: cerebral blood volume; Ctx: Cortex; Ect: Ectorhinal Ent: Entorhinal; IPN:

285 Interpeduncular nucleus; Lat: Lateral; Med: Medial; Periaq: Periaqueductal; Prim: Primary;  
 286 Sec: Secondary; Sup Coll: superior colliculus; VEH: vehicle; Vis: Visual



287  
 288 **Fig. 2: Time-dependent effects and functional connectivity analysis after atomoxetine**  
 289 **challenge**  
 290 (A) rCBV difference between atomoxetine and saline (B) Schematic representation of  
 291 changes found in (A). (C) Functional connectivity changes between atomoxetine and saline  
 292 after the pharmacological challenge in each region. Aud: Auditory; CA1, CA2, CA3: cornu  
 293 ammonis areas; CBV: cerebral blood volume; Ctx: Cortex; Ect: Ectorhinal Ent: Entorhinal;  
 294 Hip: Hippocampus; IPN: Interpeduncular nucleus; Lat: Lateral; Med: Medial; Periaq:  
 295 Periaqueductal; Prim: Primary; Sec: Secondary; Sup Coll: superior colliculus; Vis: Visual  
 296